

# Longitudinal Data and a Semantic Similarity Reward for Chest X-Ray Report Generation

Aaron Nicolson, Jason Dowling, and Bevan Koopman

The Australian e-Health Research Centre, CSIRO Health and Biosecurity, Brisbane, Australia  
{aaron.nicolson, jason.dowling, bevan.koopman}@csiro.au

## Abstract

Chest X-Ray (CXR) report generation is a promising approach to improving the efficiency of CXR interpretation. However, a significant increase in diagnostic accuracy is required before that can be realised. Motivated by this, we propose a framework that is more inline with a radiologist’s workflow by considering longitudinal data. Here, the decoder is additionally conditioned on the report from the subject’s previous imaging study via a prompt. We also propose a new reward for reinforcement learning based on CXR-BERT, which computes the similarity between reports. We conduct experiments on the MIMIC-CXR dataset. The results indicate that longitudinal data improves CXR report generation. CXR-BERT is also shown to be a promising alternative to the current state-of-the-art reward based on RadGraph. This investigation indicates that longitudinal CXR report generation can offer a substantial increase in diagnostic accuracy. Our Hugging Face model is available at: <https://huggingface.co/aehrc/cxrmate> and code is available at: <https://github.com/aehrc/cxrmate>.

## Introduction

Chest X-Ray (CXR) report generation has the potential to improve radiologist workflows (Thrall et al. 2018). While current methods are promising, a significant improvement in diagnostic accuracy is required before clinical consideration. Recent methods propose improvements to neural network architecture, training objectives, rewards for reinforcement learning, or by incorporating additional features.

However, several factors about how CXRs are interpreted in a clinical setting have been overlooked. We outline these issues—and how we address them—in Figure 1. Figure 1 A shows that an imaging study for a given subject can have multiple CXRs (e.g., frontal and lateral views). However, most methods overlook this and generate a separate report per CXR (“single-CXR” in Figure 1 B). This differs from the clinical setting where all CXRs of a study are interpreted in conjunction to produce a single report (Gaber, McGavin, and Wells 2005). Few methods replicate this and condition report generation on all CXRs of a study (“Variable-CXR” in Figure 1 C) (Miura et al. 2021). However, there has been no empirical evaluation comparing the variable-CXR case

to the single-CXR case in terms of performance. Hence, we provide this evaluation as a contribution of our study.

Returning to Figure 1 A, we note that a subject can have multiple studies over time (e.g., Study 1 and Study 2). A clinician makes use of longitudinal data by comparing the current study to previous studies and identifying differences—which can reduce interpretation difficulty (Kelly 2012). Although standard in the clinical setting, conditioning on longitudinal data has not been investigated for CXR report generation. Motivated by this, we propose longitudinal, variable-CXR report generation with the aim of improving diagnostic accuracy. Here, the decoder is conditioned on all CXRs of a subject’s current study, as well as the report from their previous study, as shown in Figure 1 D. Evidence from the MIMIC-CXR dataset to support longitudinal, variable-CXR report generation is given in Figure 2 (Johnson et al. 2019). The left plot shows that 55% of studies had multiple CXRs while the right plot shows that 50% of subjects had more than one study. This demonstrates that longitudinal data and multiple CXRs can be frequently leveraged for CXR report generation.

Finally, we also propose a reward for reinforcement learning based on CXR-BERT (Boecking et al. 2022) (a natural language understanding model specifically trained to determine the similarity between CXR reports). The choice of reward can have a large impact on performance, as demonstrated by the state-of-the-art rewards based on RadGraph (Delbrouck et al. 2022). Our reward is the cosine similarity between features of the generated and ground-truth reports, where CXR-BERT is the feature extractor. To summarise, the contributions of this study are as follows: 1) longitudinal, variable-CXR report generation via prompting the decoder with the impression section of the previous study, 2) a reward for reinforcement learning based on CXR-BERT, and 3) experimental evaluation on the MIMIC-CXR dataset, including a comparison between the single-CXR and variable-CXR cases (Johnson et al. 2019).

## Related Work

CXR report generation methods typically rely on an encoder-to-decoder model, with many recent studies proposing architectural improvements. Chen *et al.* proposed a “memory-driven” Transformer decoder (R2Gen) (Chen et al. 2020), which was later developed into a “Cross-modal

arXiv:2307.09758v1 [cs.CV] 19 Jul 2023

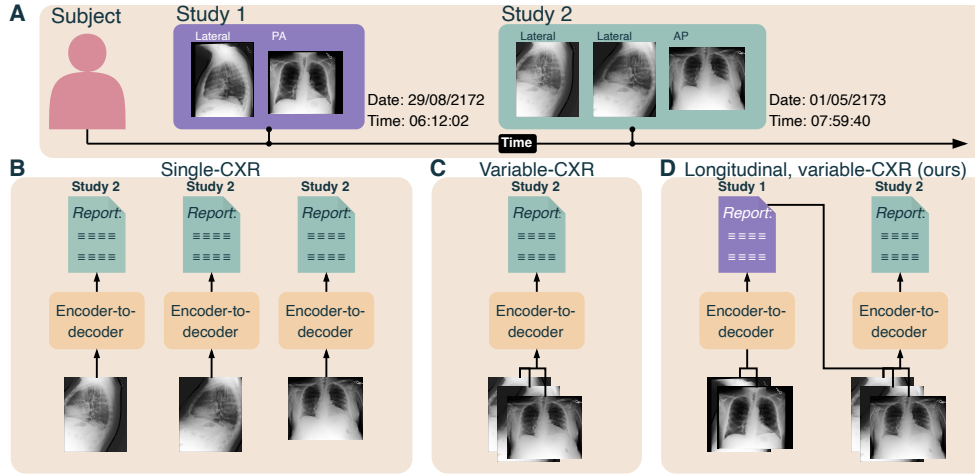


Figure 1: **A:** A subject’s imaging studies over time. CXR report generation conditioned on **B:** an individual CXR of a study, **C:** all the CXRs of a study, and **D:** all the CXRs of a study, as well as the impression section of the previous study.

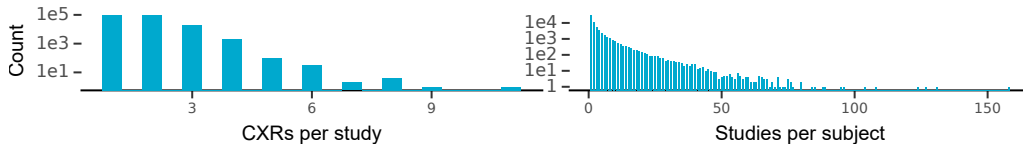


Figure 2: Histograms of the training split of MIMIC-CXR (log scale  $y$ -axis).

Memory Network” (CMN) (Chen et al. 2021). Different encoder and decoder architectures and pre-trained checkpoints were compared in (Nicolson, Dowling, and Koopman 2022), where it was found that the Convolutional vision Transformer (CvT) and DistilGPT2 performed best (CvT2DistilGPT2). You et al. proposed “align hierarchical attention”, which computes and then aligns “disease tags” and visual features from a CXR to better represent abnormal regions (You et al. 2021). Wang et al. proposed a memory-augmented sparse attention block that utilises bi-linear pooling to capture higher-order interactions between CXR features (Wang et al. 2022b). Following CvT2DistilGPT2, we use CvT as the encoder for our method. However, we use a randomly initialised Transformer decoder with a CXR report-specific tokeniser.

Others have proposed new objectives to improve the models understanding of the relationship between CXR and report (Li et al. 2022). Yan et al. proposed a Weakly-supervised Contrastive Loss (WCL) between features of the CXR and ground-truth report, where negative samples that are semantically closer to the ground-truth report are given more weight (Yan et al. 2021). Najdenkoska et al. forced features of the CXR and ground-truth report to be aligned in a latent space by formulating the report generation task as a conditional variational inference problem (Najdenkoska et al. 2021, 2022). For our method, we use the standard objectives for text-to-image generation: Teacher Forcing (TF) (Williams and Zipser 1989) and Self-Critical Sequence Training (SCST) (Rennie et al. 2017).

Some studies inject additional features into the encoder-to-decoder model. Yang et al. leveraged RadGraph (Jain et al. 2021) and retrieved reports from similar CXRs to capture “general” and “specific” knowledge about the reports, respectively (Yang et al. 2022). Wang et al. proposed several modules, such as a “knowledge graph-based task distillation module” to create a “task-aware framework” to account for the highly structured nature of reports (Wang et al. 2022a). Recently, several CXR models, including CXR report generation models, were employed to prompt ChatGPT into generating reports (Wang et al. 2023). Our method takes the novel approach of prompting the decoder with the report of the previous study, which does not require additional modules.

Rewards for SCST that are able to capture the semantic similarity between the generated and ground-truth reports have resulted in large gains. Recently, Miura et al. proposed  $\text{fact}_{\text{ENT}}$  and  $\text{fact}_{\text{ENTNLI}}$ , two rewards that take advantage of Named-Entity Recognition (NER). Here, the F1-score of the number of entity matches between the generated and ground-truth reports form the basis of the rewards (Miura et al. 2021). Delbrouck et al. proposed a set of rewards that were able to outperform  $\text{fact}_{\text{ENT}}$  and  $\text{fact}_{\text{ENTNLI}}$  using a Transformer encoder that was trained to jointly predict RadGraph entities and relations from reports (Delbrouck et al. 2022). Three rewards were formed;  $\text{RG}_{\text{E}}$  compared the entities between the generated and ground-truth reports, while  $\text{RG}_{\text{ER}}$  and  $\text{RG}_{\text{ER}}$  additionally compared the relations. In this study, we compare these to the proposed CXR-BERT

reward.

## Methods

### Longitudinal, Variable-CXR Report Generation

Longitudinal, variable-CXR report generation is defined here as conditioning the generation of a study’s report on all CXRs of a study, as well as data from previous studies. As a first step in this direction, we prompt the decoder with the report of the previous study, as shown in Figure 3. To accommodate for the prompt, we utilise four special tokens: [PMT], [PMT-SEP], [NPF], and [NPI], which denote the “prompt”, “prompt separator”, “no previous findings section” and “no previous impression section” special tokens, respectively. [NPF] and [NPI] handle cases where there is no previous study. [PMT-SEP] and [SEP] indicate the separation between the findings and impression sections for the previous and current study, respectively. Moreover, this allows the findings and impression sections to be extracted from the generated report.

When prompting the decoder, either the previous ground-truth report (“GT prompt”) or the previous generated report (“Gen. prompt”) can be used. Training with GT prompt offers a reduced training time. However, training with Gen. prompt avoids the *exposure bias* problem (Rennie et al. 2017). When training with TF, only GT prompt can be used. However, either GT prompt or Gen. prompt can be used with SCST. For SCST with Gen. prompt, we use the baseline from the preceding mini-batch update as the previous generated report. To accommodate for this, a subject’s studies must be ordered and given in subsequent mini-batches (the order of the subjects is shuffled for each epoch). When testing, the difference in performance between GT prompt and Gen. prompt can reveal how the errors in the previous generated prompt impact report generation.

### CXR-BERT Cosine Similarity Reward

CXR-BERT is a Transformer encoder pre-trained in various stages on PubMed abstracts, clinical notes from MIMIC-III (Johnson et al. 2016), as well as reports from MIMIC-CXR, which we denote as  $E(\cdot)$  (Boecking et al. 2022). It has two pre-training tasks, with one being Radiology Section Matching (RSM). For RSM, the output feature vector for the [CLS] special token of CXR-BERT ( $[E(\cdot)]_{[\text{CLS}]}$ ) and a two-layer feedforward neural network ( $P(\cdot)$ ) are used in series to compute features of the findings and impression sections. During training, a contrastive loss forces the findings and impression section features from the same report to have a higher similarity, while those from different reports to have a lower similarity.

We leverage CXR-BERT as a reward for SCST; instead of sections, we compute the similarity between the generated and ground-truth reports (which include both the findings and impression sections). Let  $\mathbf{w}^{\text{gen}} = (w_1^{\text{gen}}, \dots, w_M^{\text{gen}})$  and  $\mathbf{w}^{\text{gt}} = (w_1^{\text{gt}}, \dots, w_N^{\text{gt}})$  denote the vectors of  $M$  and  $N$  tokens of the generated and ground-truth reports, respectively. For SCST, the generated report is either the sample or the baseline. Features for both reports are then computed as:  $\mathbf{t}^{\text{gen}} =$

$P([E(\mathbf{w}^{\text{gen}})]_{[\text{CLS}]})$  and  $\mathbf{t}^{\text{gt}} = P([E(\mathbf{w}^{\text{gt}})]_{[\text{CLS}]})$ . Their cosine similarity gives the reward:  $r = (\mathbf{t}^{\text{gen}} \cdot \mathbf{t}^{\text{gt}}) / (\|\mathbf{t}^{\text{gen}}\| \cdot \|\mathbf{t}^{\text{gt}}\|)$ .

### Experiment Setup

**Dataset formatting:** The MIMIC-CXR dataset was used for evaluation (Johnson et al. 2019). Sections from the ground-truth reports were obtained using the official text extraction tool.<sup>1</sup> Studies with either a missing findings or impression section, and studies with more than five CXRs per study were removed. This gave a training/validation/test split of 57 098/436/280 subjects, 125 395/991/1 624 studies, and 232 715/1 837/2 872 CXRs. Minimal formatting was applied to the ground-truth reports; newline characters, tab characters, and consecutive white spaces were replaced with a single white-space character. The ground-truth reports were not truncated during training or testing. The order of a subject’s studies was determined by the date and time provided with the metadata. The date and time for studies 57 077 869 and 58 837 588 of subject 15 964 158 were identical, making it impossible to determine their order. Hence, these studies, along with all of their subsequent studies were removed from the training set for the longitudinal case only, reducing the training set size to 125 384 studies and 232 692 CXRs.

**Model:** CvT was the encoder (specifically, CvT-21 pre-trained on ImageNet-22K and fine-tuned on ImageNet-1K at a resolution of  $384 \times 384$ ) (Wu et al. 2021; Nicolson, Dowling, and Koopman 2022). Layer normalisation was applied to its last hidden state, followed by a projection to the decoder’s hidden size. The encoded features for each CXR were concatenated and fed to the cross-attention of the decoder. Each CXR was resized using bilinear interpolation so that its smallest side had a length of 384 and its largest side maintained the aspect ratio. Next, the resized CXR was cropped to a size of  $\mathbb{R}^{3 \times 384 \times 384}$ . The crop location was random during training and centred during testing. During training, the CXR was rotated around its centre where the angle of rotation was sampled from  $\mathcal{U}[-5^\circ, 5^\circ]$ . Finally, the CXR was standardised using the statistics provided with the CvT-21 checkpoint. For the decoder, a byte-level byte pair encoding tokeniser (Wang, Cho, and Gu 2020) was trained on the findings and impression sections of the training set (with a vocabulary size of 30 000). The BERT<sub>BASE</sub> architecture was employed as the decoder, as it is equipped with section embeddings. The decoder had six layers, was randomly initialised, included a language model head, and had a vocabulary size of 30 000. For the longitudinal case, we found that training the described model on the longitudinal, variable-CXR report generation task would not result in an improvement over the variable-CXR case. To ease the difficulty of learning this task, we adapt the trained variable-CXR model to the task of longitudinal, variable CXR report generation using Low Rank Approximation (LoRA) (Hu et al. 2022). LoRA is applied to the query and key weights of each self-attention head of the decoder with a rank of eight, an alpha of 32, and a dropout rate of 0.1. LoRA adds 147K parameters to the 80.8M parameters of the model, where all non-LoRA

<sup>1</sup><https://github.com/MIT-LCP/mimic-cxr/tree/master/txt>

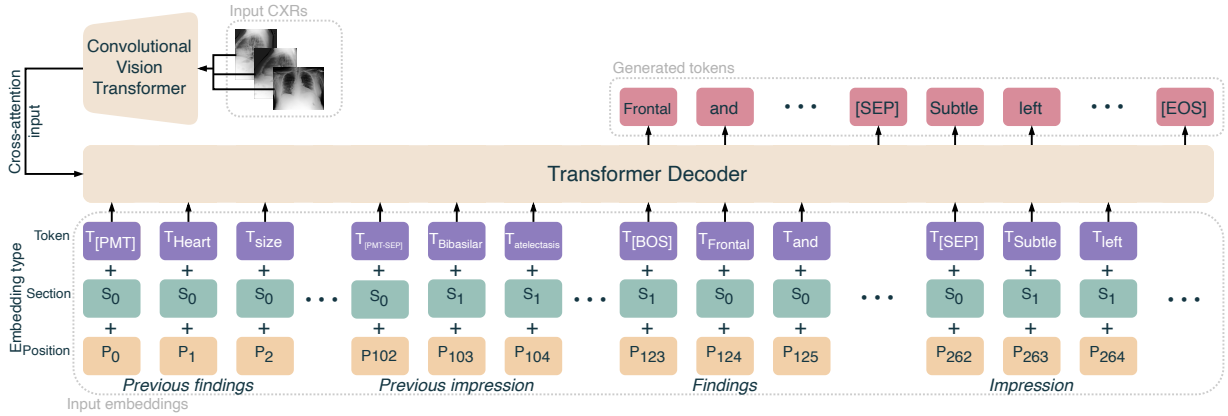


Figure 3: The proposed longitudinal, variable-CXR report generator that is prompted by the impression section of the previous study. [BOS] and [EOS] denote the “beginning-of-sentence” and “end-of-sentence” special tokens, respectively.

parameters are frozen during fine-tuning. Greedy search and beam search with four beams were employed during validation and testing, respectively. If the previous study was not available or had been removed, the [NPF] and [NPI] tokens were used.

**Training:** Two stages of training were performed: TF, followed by SCST. Gradient descent optimisation was performed with AdamW (Loshchilov and Hutter 2022) at an initial learning rate of  $5e-5$  for TF and  $5e-6$  for SCST, a mini-batch size of 32, 32 epochs for TF, and 1 epoch for SCST. For SCST, validation was performed every  $\frac{1}{10}$  of an epoch. The validation macro-averaged CheXbert F1 (for both the findings and impression sections) was the monitored metric for checkpoint selection. For SCST, the baseline was generated with greedy search, while the sample was produced with top- $k$  sampling ( $k = 50$ ). During SCST, the encoder was frozen, while all parameters of the decoder were learnable (both LoRA and non-LoRA parameters). The maximum number of tokens for TF, the generated report, and the prompt was 256 each.

**Comparison methods:** We compared the CXR-BERT reward to other rewards: CIDEr (Vedantam, Lawrence Zitnick, and Parikh 2015), Clinical Correctness Reward (CCR) (with CheXbert instead of CheXpert) (Liu et al. 2019),  $fact_{ENTNLI}$  and  $fact_{ENTNLI} + BERTScore$  (Miura et al. 2021), as well as  $RG_E$ ,  $RG_{ER}$  and  $RG_{\overline{ER}}$  (Delbrouck et al. 2022). Moreover, we compared our CXR report generator to others in the literature that had open-source code and an available trained model. These included R2Gen (Chen et al. 2020),  $M^2 fact_{ENT}$  and  $M^2 fact_{ENTNLI}$  (Miura et al. 2021), WCL (Yan et al. 2021), CMN (Chen et al. 2021), and CvT2DistilGPT2 (the MIMIC-CXR SCST checkpoint) (Nicolson, Dowling, and Koopman 2022).

**Metrics:** Several metrics were used for evaluation:  $RG_{ER}$ , CXR-BERT (described in Subsection ), METEOR (M) (Banerjee and Lavie 2005), ROUGE-L (R-L) (Lin and Och 2004), and CIDEr (C) (Vedantam, Lawrence Zitnick, and Parikh 2015). For the single-CXR case, we average the scores over all reports for a study to compare to the variable-

CXR case. We perform statistical testing; first, a Levene’s test revealed that the variances across methods were not homogeneous. Next, a one-way Welch’s ANOVA determined that there was a significant difference between methods. Finally, Games-Howell post hoc tests were used for pairwise testing. The reported scores are the average over all studies. We also used the macro-averaged F1, Precision (P), and Recall (R) over the 14 CheXbert classes as a metric (Smit et al. 2020). “No mention”, “negative”, and “uncertain” were considered negative, while “positive” was considered positive. Here, the true positives, false positives, and false negatives were averaged over the reports of each study for the single-CXR case. No statistical testing was performed for CheXbert.

## Results & Discussion

The results for single, variable, and longitudinal CXR report generation trained with TF are shown in Figure 4 (for both the findings and impression sections). The difference between Gen prompt and GT prompt is not statistically significant, indicating that Gen prompt does not hinder generation. Both longitudinal cases outperform the variable and single-CXR cases, indicating that leveraging longitudinal data improves CXR report generation. Moreover, the variable-CXR case outperforms the single-CXR case, indicating that conditioning on all CXRs of a study (which may contain multiple views) improves CXR report generation.

The results for each reward are given in Figure 5 (for both the findings and impression sections). Each longitudinal, variable-CXR report generator was trained with GT prompt, except for “CXR-BERT (Gen prompt)”. The performance improvement of CXR-BERT (Gen prompt) over CXR-BERT is statistically significant, and can be attributed to avoiding exposure bias. CXR-BERT and  $RG_{ER}$  performed best on the corresponding metrics that they were optimised on. However, CXR-BERT attained the highest CheXbert F1 and METEOR scores. This indicates that rewarding based on similar latent alignments with CXR-BERT

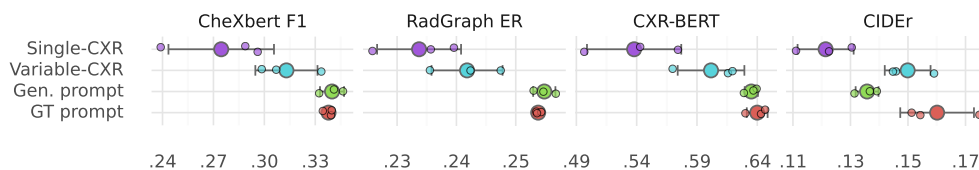


Figure 4: Results for the different strategies of Figure 1. The large dots and error bars indicate the mean and standard deviation over three training runs, respectively. Dotted lines indicate a statistically significant difference ( $p < 0.05$ ,  $n = 4872$ ).

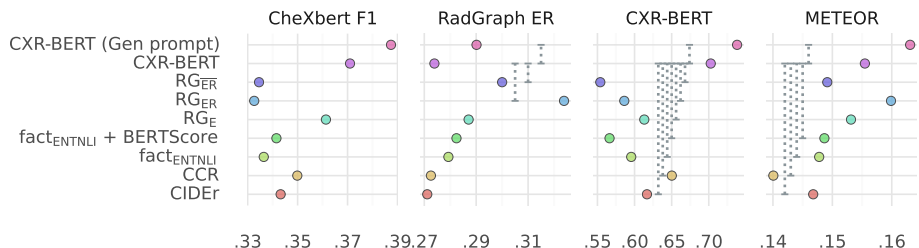


Figure 5: Results for each reward with the longitudinal, variable-CXR report generator. Dotted lines indicate a stat. sig. difference to CXR-BERT ( $p < 0.05$ ,  $n = 1624$ ).

is a promising alternative to rewarding based on matching entities and relations with  $R_{G_{ER}}$ .

In Table 1, our longitudinal, variable-CXR report generator trained with the CXR-BERT (Gen prompt) reward, which we name CXRMate, is compared to other methods in the literature. For methods that generate both the findings and impression section, CXRMate attained the highest score for each metric (except CheXbert P). The low performance of R2Gen, WCL, CMN, and CvT2DistilGPT2 could be attributed to being conditioned on a single CXR, not being trained with SCST (except CvT2DistilGPT2), and being trained on the truncated ground-truth reports of Chen *et al.* (Chen et al. 2020).

$M^2 \text{ fact}_{ENT}$  and  $M^2 \text{ fact}_{ENTNLI}$  both solely generate the findings section, were conditioned on a variable number of CXRs, and trained with NER-based rewards. These are strong benchmarks. While CXRMate produced the highest F1, R and CXR-BERT scores, it was outperformed on the remaining metrics. The performance deficit could be caused by multiple factors. First, CXRMate was optimised to generate both the findings and impression sections, which could reduce its performance when only generating the findings section. Second, the  $M^2$  architecture could be superior to the CXRMate encoder-to-decoder model. The performance of  $M^2 \text{ fact}_{ENTNLI}$  on  $R_{G_{ER}}$  could be due to its  $\text{fact}_{ENTNLI} + \text{BERTScore}$  reward being more similar to  $R_{G_{ER}}$  than CXR-BERT.

## Conclusion

In this work, we investigated longitudinal, variable-CXR report generation. Our proposed framework more closely aligns with the clinical setting; it accounts for a variable number of CXRs and longitudinal data from previous studies. An empirical evaluation on MIMIC-CXR shows that generating a single report conditioned on all CXRs of a subject’s study is superior to generating a report for each

CXR. Moreover, prompting the decoder with the impression section from the report of the previous study offers a further improvement in performance. Finally, we show that CXR-BERT is a promising reward for CXR report generation and SCST. Future work could consider other longitudinal data, as well as different schema to incorporate longitudinal data. A more thorough experimental investigation is required with a study on the impact of longitudinal data on different pathologies, an evaluation on external datasets, and a subjective evaluation with clinicians. Incorporating longitudinal data could be a path forward to increasing the diagnostic accuracy of CXR report generation.

## References

- Banerjee, S.; and Lavie, A. 2005. METEOR: An Automatic Metric for MT Evaluation with Improved Correlation with Human Judgments. In *ACL Workshops*, 65–72.
- Boecking, B.; Usuyama, N.; Bannur, S.; Castro, D. C.; Schwaighofer, A.; Hyland, S.; Wetscherek, M.; Naumann, T.; Nori, A.; Alvarez-Valle, J.; Poon, H.; and Oktay, O. 2022. Making the Most of Text Semantics to Improve Biomedical Vision–Language Processing. In *ECCV*, 1–21.
- Chen, Z.; Shen, Y.; Song, Y.; and Wan, X. 2021. Cross-modal Memory Networks for Radiology Report Generation. In *IJCNLP*, 5904–5914.
- Chen, Z.; Song, Y.; Chang, T.-H.; and Wan, X. 2020. Generating Radiology Reports via Memory-driven Transformer. In *EMNLP*, 1439–1449.
- Delbrouck, J.-B.; Chambon, P.; Bluethgen, C.; Tsai, E.; Al-musa, O.; and Langlotz, C. 2022. Improving the Factual Correctness of Radiology Report Generation with Semantic Rewards. In *EMNLP*, 4348–4360.
- Gaber, K. A.; McGavin, C. R.; and Wells, I. P. 2005. Lateral Chest X-Ray for Physicians. *Journal of the Royal Society of Medicine*, 98(7): 310–312.

Table 1: Comparison to other methods. (\*) Significant ( $p < 0.05$ ,  $n = 1\ 624$ ).

Model	CheXbert			R <sub>GER</sub>	CXR-BERT	M	R-L	C
	F1	P	R					
<i>Findings and impression</i>								
R2Gen (Chen et al. 2020)	0.164	0.386	0.154	0.196	0.349	0.113	0.212	0.071
WCL (Yan et al. 2021)	0.219	0.360	0.205	0.205	0.436	0.117	0.213	0.069
CMN (Chen et al. 2021)	0.256	0.378	0.250	0.218	0.461	0.116	0.218	0.074
CvT2DistilGPT2 (Nicolson, Dowling, and Koopman 2022)	0.260	<b>0.447</b>	0.249	0.219	0.577	0.118	0.222	0.090
<b>CXRMate (ours)</b>	<b>0.387</b>	0.415	<b>0.417</b>	<b>0.290*</b>	<b>0.738*</b>	<b>0.163*</b>	<b>0.242*</b>	<b>0.128*</b>
<i>Findings</i>								
$\mathcal{M}^2$ fact <sub>ENT</sub>	0.235	0.381	0.244	0.237	0.553	0.121	0.207	0.133
$\mathcal{M}^2$ fact <sub>ENTNLI</sub>	0.311	<b>0.412</b>	0.329	<b>0.320*</b>	0.681	<b>0.169</b>	<b>0.269*</b>	<b>0.187*</b>
<b>CXRMate (ours)</b>	<b>0.360</b>	0.384	<b>0.394</b>	0.280	<b>0.731*</b>	0.167	0.244	0.145

Hu, E. J.; yelong shen; Wallis, P.; Allen-Zhu, Z.; Li, Y.; Wang, S.; Wang, L.; and Chen, W. 2022. LoRA: Low-Rank Adaptation of Large Language Models. In *International Conference on Learning Representations*.

Jain, S.; Agrawal, A.; Saporta, A.; Truong, S. Q.; Nguyen Duong, D.; Bui, T.; Chambon, P.; Lungren, M.; Ng, A.; Langlotz, C.; and Rajpurkar, P. 2021. RadGraph: Extracting Clinical Entities and Relations from Radiology Reports. *PhysioNet*.

Johnson, A. E. W.; Pollard, T. J.; Greenbaum, N. R.; Lungren, M. P.; Deng, C.-y.; Peng, Y.; Lu, Z.; Mark, R. G.; Berkowitz, S. J.; and Horng, S. 2019. MIMIC-CXR-JPG, a large publicly available database of labeled chest radiographs. *PhysioNet*.

Johnson, A. E. W.; Pollard, T. J.; Shen, L.; Lehman, L.-w. H.; Feng, M.; Ghassemi, M.; Moody, B.; Szolovits, P.; Anthony Celi, L.; and Mark, R. G. 2016. MIMIC-III, a freely accessible critical care database. *Scientific Data*, 3(1): 160035.

Kelly, B. 2012. The chest radiograph. *The Ulster Medical Journal*, 81(23620614): 143–148.

Li, J.; Li, S.; Hu, Y.; and Tao, H. 2022. A Self-guided Framework for Radiology Report Generation. In *MICCAI*, 588–598.

Lin, C.-Y.; and Och, F. J. 2004. Automatic Evaluation of Machine Translation Quality Using Longest Common Subsequence and Skip-Bigram Statistics. In *ACL*, 605–612.

Liu, G.; Hsu, T.-M. H.; McDermott, M.; Boag, W.; Weng, W.-H.; Szolovits, P.; and Ghassemi, M. 2019. Clinically accurate chest X-ray report generation. In *MLHC*, 249–269.

Loshchilov, I.; and Hutter, F. 2022. Decoupled Weight Decay Regularization. In *ICLR*.

Miura, Y.; Zhang, Y.; Tsai, E.; Langlotz, C.; and Jurafsky, D. 2021. Improving Factual Completeness and Consistency of Image-to-Text Radiology Report Generation. In *NAACL*, 5288–5304.

Najdenkoska, I.; Zhen, X.; Worring, M.; and Shao, L. 2021. Variational Topic Inference for Chest X-Ray Report Generation. In *MICCAI*, 625–635.

Najdenkoska, I.; Zhen, X.; Worring, M.; and Shao, L. 2022. Uncertainty-aware report generation for chest X-rays by variational topic inference. *Medical Image Analysis*, 82: 102603.

Nicolson, A.; Dowling, J.; and Koopman, B. 2022. Improving Chest X-Ray Report Generation by Leveraging Warm-Starting. *ArXiv:2201.09405 [cs.CV]*.

Rennie, S. J.; Marcheret, E.; Mroueh, Y.; Ross, J.; and Goel, V. 2017. Self-Critical Sequence Training for Image Captioning. In *CVPR*, 1179–1195.

Smit, A.; Jain, S.; Rajpurkar, P.; Pareek, A.; Ng, A.; and Lungren, M. 2020. Combining Automatic Labelers and Expert Annotations for Accurate Radiology Report Labeling Using BERT. In *EMNLP*, 1500–1519.

Thrall, J. H.; Li, X.; Li, Q.; Cruz, C.; Do, S.; Dreyer, K.; and Brink, J. 2018. Artificial Intelligence and Machine Learning in Radiology: Opportunities, Challenges, Pitfalls, and Criteria for Success. *Journal of the American College of Radiology*, 15(3): 504–508.

Vedantam, R.; Lawrence Zitnick, C.; and Parikh, D. 2015. CIDEr: Consensus-Based Image Description Evaluation. In *CVPR*, 4566–4575.

Wang, C.; Cho, K.; and Gu, J. 2020. Neural machine translation with byte-level subwords. In *AAAI*, 9154–9160.

Wang, L.; Ning, M.; Lu, D.; Wei, D.; Zheng, Y.; and Chen, J. 2022a. An Inclusive Task-Aware Framework for Radiology Report Generation. In *MICCAI*, 568–577.

Wang, S.; Zhao, Z.; Ouyang, X.; Wang, Q.; and Shen, D. 2023. ChatCAD: Interactive Computer-Aided Diagnosis on Medical Image using Large Language Models. *ArXiv:2302.07257 [cs.CV]*.

Wang, Z.; Tang, M.; Wang, L.; Li, X.; and Zhou, L. 2022b. A Medical Semantic-Assisted Transformer for Radiographic Report Generation. In *MICCAI*, 655–664.

Williams, R. J.; and Zipser, D. 1989. A Learning Algorithm for Continually Running Fully Recurrent Neural Networks. *Neural Computation*, 1(2): 270–280.

Wu, H.; Xiao, B.; Codella, N.; Liu, M.; Dai, X.; Yuan, L.; and Zhang, L. 2021. CvT: Introducing Convolutions to Vision Transformers. In *ICCV*, 22–31.

Yan, A.; He, Z.; Lu, X.; Du, J.; Chang, E.; Gentili, A.; McAuley, J.; and Hsu, C.-N. 2021. Weakly Supervised Contrastive Learning for Chest X-Ray Report Generation. In *EMNLP*, 4009–4015.

Yang, S.; Wu, X.; Ge, S.; Zhou, S. K.; and Xiao, L. 2022. Knowledge matters: Chest radiology report generation with general and specific knowledge. *Medical Image Analysis*, 80: 102510.

You, D.; Liu, F.; Ge, S.; Xie, X.; Zhang, J.; and Wu, X. 2021. AlignTransformer: Hierarchical Alignment of Visual Regions and Disease Tags for Medical Report Generation. In *MICCAI*, 72–82.